Research Article | Vol. 31, No. 12 / 5 Jun 2023 / Optics Express 19554
Optics EXPRESS

Spectral broadening in convex-concave multipass cells

VICTOR HARITON,[1,2,*] KILIAN FRITSCH,[1,4] KEVIN SCHWARZ,[1,5] NAZAR KOVALENKO,[1,6] GONÇALO FIGUEIRA,[2,7] GUNNAR ARISHOLM,[3,8] AND OLEG PRONIN[1,9]

[1]*Helmut-Schmidt-Universität / Universität der Bundeswehr Hamburg, Holstenhofweg 85, D-22043 Hamburg, Germany*
[2]*Instituto Superior Técnico, Universidade de Lisboa, Av. Rovisco Pais no1, 1049-001 Lisboa, Portugal*
[3]*FFI (Norwegian Defence Research Establishment), Postboks 25, NO-2027 Kjeller, Norway*
[4]*kilian.fritsch@hsu-hh.de*
[5]*kevin.schwarz@hsu-hh.de*
[6]*nazar.kovalenko@hsu-hh.de*
[7]*goncalo.figueira@ist.utl.pt*
[8]*gunnar.arisholm@ffi.no*
[9]*oleg.pronin@hsu-hh.de*
[*]*victor.hariton@ist.utl.pt*

Abstract: Since its first demonstration in 2016, the multi-pass spectral broadening technique has covered impressive ranges of pulse energy (3 µJ – 100 mJ) and peak power (4 MW – 100 GW). Energy scaling of this technique into the joule-level is currently limited by phenomena such as optical damage, gas ionization and spatio-spectral beam inhomogeneity. These limitations can be overcome by the novel multi-pass convex-concave arrangement, which exhibits crucial properties such as large mode size and compactness. In a proof-of-principle experiment, 260 fs, 15 µJ and 200 µJ pulses are broadened and subsequently compressed to approximately 50 fs with 90% efficiency and excellent spatio-spectral homogeneity across the beam profile. We simulate the proposed concept for spectral broadening of 40 mJ and 1.3 ps input pulses and discuss the possibility of further scaling.

1. Introduction

High energy, high-peak power ultrafast lasers are in demand for many applications such as laser-based plasma accelerators as well as particle, THz and X-ray sources [1]. In particular, high repetition rates and short pulse durations are sought after [1]. These are needed to make laser plasma accelerators compatible with real-world applications, and to improve existing scientific applications, for example, to push the cut-off wavelength of high-harmonic generation beyond the water-window and advance attosecond science. Industrial applications call for reasonable wall-plug efficiency and maintenance costs of their laser systems. This, in turn, implies the use of Yb-based, diode-pumped platforms. However, these laser systems are intrinsically limited in the shortest pulse duration achievable by the narrow bandwidth of the emission cross-section, requiring an external mechanism to shorten the pulses below the sub-ps level. Nonlinear spectral broadening via self-phase modulation (SPM) followed by pulse compression is a well-established approach. Different concepts can be used to execute this method, such as free propagation in bulk or thin multi-plates, solid- or hollow-core fibers, and multipass cells [2–4]. Scaling these techniques toward high energy and high average power lasers is an ongoing research challenge. Free propagation in single and multi-plate was scaled towards the J-level pulse energy range [5–8].

#486797 https://doi.org/10.1364/OE.486797
Journal © 2023 Received 31 Jan 2023; revised 30 Mar 2023; accepted 31 Mar 2023; published 26 May 2023

Optics EXPRESS

However, these approaches require clean flat-top beam profiles to avoid self-focusing and spectral inhomogeneities. Waveguides possess several advantages and can be reliably employed as a post-compression technique up to tens of millijoules [9,10]. In particular, using this technique the first isolated attosecond pulses were created [11], however, due to intrinsic small beam size necessity, it generally complicates the handling of high-average-power sources operating at high repetition rate. A good summary and analysis of the existing post-compression techniques can be found in [12,13]. The multipass cells provide an alternative method for SPM-based spectral broadening with many new possibilities such as dispersion engineering, huge peak-, and average-power adaptability, and scalability [3,12,14–16]. The technique is based on free-space propagation through a nonlinear medium (either dielectric bulk material or gases) in a multi-pass or quasi-waveguide arrangement [17]. The multi-pass setup repeatedly generates foci with sufficient intensity to accumulate SPM, while simultaneously distributing the nonlinear phase shifts over multiple passes with intermittent free-space propagation in the quasi-waveguide, which supresses the self-focusing and its detrimental effects. Dispersion compensation within the multi-pass arrangement as well as subsequent chirp removal of the SPM-induced phase leads to a temporal compression of the output pulses and it has been demonstrated down to a few-cycle pulses [18–21].

The highest energies at which this method has been successfully applied are 40 mJ, 5 kHz, 1.3 ps pulses compressed to 34 fs, and 112 mJ, 1.3 ps pulses spectrally broadened to an equivalent 37 fs Fourier-transform limit [15,22–24]. The applicability of the multi-pass method in the high-energy range is mainly limited by two detrimental effects: laser-induced damage of optical surfaces and ionization of the nonlinear material [25]. At high peak power levels ($>10^{12}$ W), ionization is currently the main bottleneck preventing further scaling [23]. So far, most of multi-pass cells implemented for the broadening experiments use a Herriott-cell (HC) arrangement with two concave mirrors (cav-cav configuration). The properties of their eigenmodes are determined by the radii of curvature (ROC) of each mirror and their separation. Increasing both parameters scales up the focus size with the square root of the cell length and thereby avoids ionization, although at the cost of an extremely large setup spanning up to ten meters [22,24].

HCs are similar in nature to optical resonators and are normally designed by using two concave mirrors. However, convex-concave (vex-cav) configurations can also be realized and can be similarly derived using the same equations as for concave-concave cells (see Appendix A and B) and, in general, for any other stable resonator configuration. This alternative configuration is characterized by its large mode volume [26]. This would allow an increase of the input energies toward values that were not achievable previously. No foci are present in the vex-cav multi-pass cell arrangement, which mitigates the ionization problem. In this configuration, virtual foci are located outside the cell behind the convex mirror M2 (see Fig. 1). Besides lowering the peak intensity and thus avoiding ionization, the lack of foci allows the setup to be folded multiple times, decreasing its length and making it manageable for practical applications. The folding is possible since the point of highest fluence is on the convex cell mirror, therefore a folding mirror may be inserted anywhere in the cell and experience lower fluences.

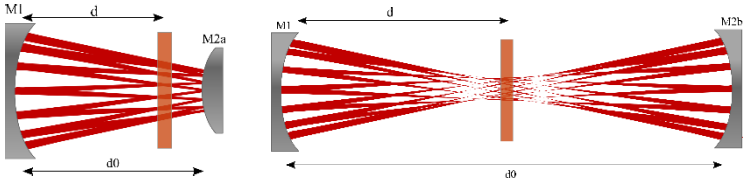

Fig. 1. Schematic side view of a: a) vex-cav Herriott-type multi-pass cell and b) cav-cav multipass cell. Mirror M2a (shown here) corresponds to the convex mirror and M2b to the concave option, respectively, while M1 remains unchanged.

Optics EXPRESS

The vex-cav geometry was previously suggested for nonlinear multi-pass cells [25] with the emphasis on their spatio-temporal coupling, however, experimentally it was not realized. Here we experimentally demonstrate that the vex-cav configuration has excellent spectral homogeneity in the output beam, comparable to the well-established cav-cav arrangements. This work is the continuation of our patent [27] which showed the first proof of principle experimental demonstration of this concept.

2. Convex-concave setup

The goal of this work is to provide experimental evidence that the novel convex-concave configuration can be employed for spectral broadening and pulse compression and provide similar results as the traditional concave-concave cells. To demonstrate it, an experimental comparison is conducted between the spectral broadening and compression results obtained with both HC geometries. The two HC schematics are depicted in Fig. 1 and Table 1 outlines the main parameters used and the results obtained in both configurations.

Table 1. Parameters used for spectral broadening in convex-concave and concave-concave cells.[a]

Vex-Cav cell	Eigenmode VC	Cav-Cav cell	Eigenmode CC	Input pulse
R_1 -200 mm	w_1 336 µm	R_1 -200 mm	w_1 358 µm	E_p 15 µJ
R_2 + 250 mm	w_2 182 µm	R_2 -250 mm	w_2 471 µm	P_{peak} 54×10^6 W
L_{cell} 114 mm	w_{egn} 170 µm	L_{cell} 378 mm	w_{egn} 164 µm	τ_{fwhm} 260×10^{-15} s
M_{rt} 4	$F_{peak\ (on\ M2)}$ 2.9 mJ cm^{-2}	M_{rt} 14	$F_{peak\ (on\ M1)}$ 0.8 mJ cm^{-2}	λ_0 1030 nm
N_{rt} 19	I_{peak} 100 GWcm^{-2}	N_{rt} 19	I_{peak} 130 GWcm^{-2}	P_{peak}/P_{crit} ~14
η [%] ~91	B_{int} 0.51 rad	η [%] ~90	B_{int} 0.5 rad	Thickness FS 3 mm

[a] R_i: ROC of cavity mirror i = 1, 2; L_{cell}: total cell length; M_{rt}: cell configuration number (see Appendix B); N_{rt}: number of roundtrips; η : efficiency; (eigenmode) w_i: beam width on cavity mirror i = 1, 2; w_{egn}: eigenmode waist in the focus; B_{int}: B-integral per pass; I_{peak},F_{peak}: peak intensity and fluence. (input pulse) E_p,P_{peak}, τ_{fwhm}, λ_0, P_{peak}/P_{crit}: input pulse energy, peak power, duration, central wavelength and peak over critical power ratio.

The vex-cav multipass cell was designed to broaden the output pulses from a commercial laser (Light Conversion Pharos) delivering 15 W average power and 260 fs FWHM pulse duration at 1 MHz repetition frequency, corresponding to 56.4 MW peak power. A broadening factor of 5 was chosen due to a simple one-stage implementation and the possibility of comparison with the previously demonstrated configurations showing similar broadening factors [2,314]. The broadening setup consists of two HC mirrors and a fused silica (FS) plate for the nonlinear broadening medium. The left mirror (M1) is spherically concave with a -200 mm radius of curvature and 50.8 mm diameter. The right mirror (M2a) is spherically convex with a + 250 mm ROC and 25.4 mm diameter. M1 has a dispersive coating introducing -140 fs^2 group delay dispersion (GDD) per reflection, in order to compensate the dispersion of the 3 mm thick FS plate. The coating on M2a is highly reflective (HR) with nearly zero dispersion. The separation between the two mirrors is adjusted to 114 mm, providing 19 reflections per mirror and 38 passes through the anti-reflective (AR) coated FS plate. The input and output coupling is performed by a rectangular scraper mirror in front of M1. The Gaussian eigenmode of the cell is defined by a beam radius of 336 µm on M1 and w_2 = 182 µm on M2a. The laser mode is matched to the HC eigenmode by a Galilean-type beam expander. The FS plate is located at a distance d = 110 mm from M1. The eigenmode has a beam radius of w = 193 µm at this position (see Fig. 1).

The broadened output spectrum spans from 990 nm to 1070 nm (Fig. 2(a)), shaded area) with a corresponding Fourier-transform limit (FTL) of 49 fs, which amounts to a compression factor of 5.5. Pulse compression is achieved by six dispersive mirrors with -400 fs^2 GDD each, resulting in a measured pulse duration of 53 fs FWHM (Fig. 2(b)), solid line), with a transmission

Optics EXPRESS

efficiency through the HC and the compression stage of 91%. Over 80% of the remaining energy is contained in the main pulse, as shown by the retrieved trace of a frequency-resolved optical gating (FROG) device (pulseCheck 15, APE GmbH). A small second order chirp is still present, however with mirrors delivering -400fs^2 it could not be completely compensated. Using mirrors with less GDD per bounce could improve the compression and potentially get closer to the FTL duration. The FROG device was not synchronized to the pulse train from Pharos laser which could have caused the modulation pattern in the measured FROG traces. However, the results were verified with a commercial autocorrelator and present good agreement.

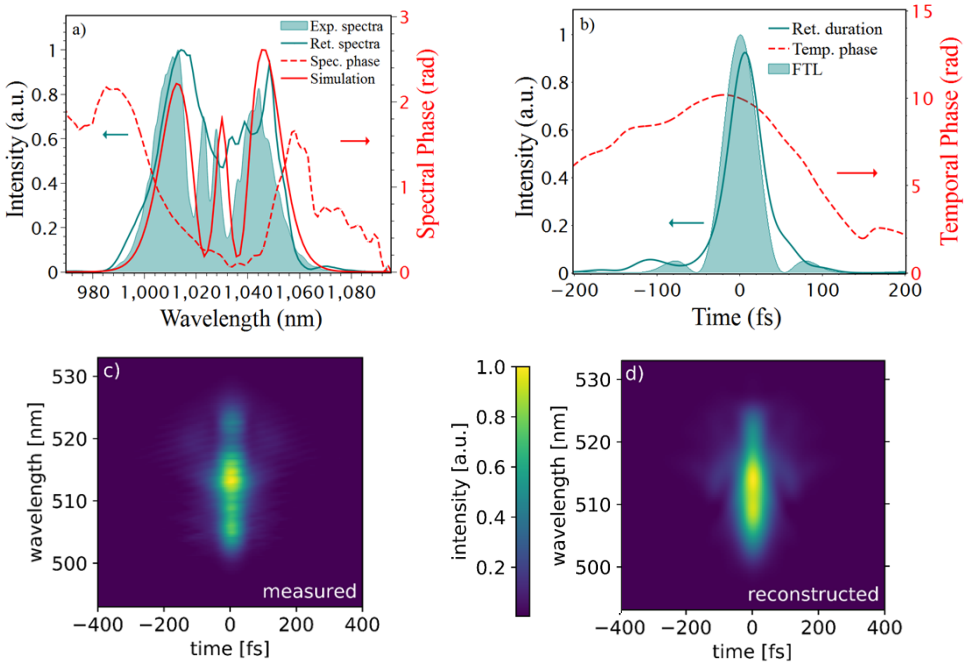

Fig. 2. a) Measured (shaded area), simulated (red line) and FROG-retrieved (green line) output spectrum and reconstructed spectral phase (dashed line) for the concave-convex configuration at an input energy of 15 µJ. The FROG error is 7×10^{-3} on a 256×256 grid. b) FROG-retrieved temporal profile (solid line), temporal phase profile (dashed line) and FTL reference (shaded area). Measured duration of 53 fs with a FTL of 49 fs. c) Measured and d) retrieved FROG traces.

In order to cross-check the experimental results with the vex-cav geometry, numerical simulations of nonlinear pulse propagation are conducted with the SISYFOS [28] code, which includes both transverse dimensions and the Kerr effect presented in the FS plate. The spatial grid was restricted to a single quadrant by exploiting the mirror symmetry of the beam. The code has been previously benchmarked and was applied to bulk and multi-pass cell (MPC) broadening simulations [29–31] in different energy ranges and configurations. The simulation results are shown in Fig. 2; it uses a nonlinear refractive (n_2) index of 2.3×10^{-20} m^2/W for the FS plate and assumes vacuum between the cell mirrors, neglecting the air nonlinearity. The code predicts accurately the amount of broadening and the output duration from this configuration.

In contrast to the single-pass broadening [32,33] the multi-pass broadening accumulates the nonlinear phase shift over many passes, overcomes the onset of self-focusing, and thus provides excellent spatio-spectral homogeneity of the output beam. The onset of inhomogeneous broadening manifests itself as a strong variation of the spectral shape across the radial beam profile, leading to a significant beam quality deterioration [32,33]. Numerical simulations

Optics EXPRESS

performed for cav-cav configurations show that the expected beam quality factor M^2 strongly depends on the acquired nonlinear phase φ after the bulk spectral broadening [17,14, 34,35]. Therefore, in a multi-pass geometry, a low peak nonlinear phase-shift per pass through the nonlinear medium is essential for high throughput efficiency and high beam quality [2]. In the current setup, a nonlinear phase of $\varphi \approx 0.25$ rad per pass is adopted while the gas-filled multi-pass cells can tolerate up to 1 rad per pass [23].

A 400 µm core diameter multi-mode fiber is used to scan over the beam with a step size of 0.2 mm, using the procedure described in [4]. The spectra were recorded with a spectrometer (Ocean Optics Flame-T series) and for each measurement $I_\lambda(\lambda)$ the overlapping percentage with the central intensity spectra $I_\lambda^{ref}(\lambda)$ (spectrum in the centre of the beam) was calculated, according to the following formula:

$$V = \left[\int \sqrt{I_\lambda(\lambda) * I_\lambda^{ref}(\lambda)}\, d\lambda\right]^2 \left[\int I_\lambda(\lambda) d\lambda \int I_\lambda^{ref}(\lambda) d\lambda\right]^{-1} \quad (1)$$

The results for both axes are plotted in Fig. 3. The homogeneity is additionally quantified by means of the intensity weighted overlap average $V_{avg} = \sum I \times V / \sum I$ [4]. We obtain $V_x^{avg} = 99\%$ and $V_y^{avg} = 98\%$ for the tangential and sagittal directions respectively, which are comparable to state-of-the-art cav-cav systems with similar broadening factors in bulk material. Moreover, the spectral overlap exceeds 90% in the beam diameter of ~3 mm defined as $1/e^2$, which indicates a remarkable homogeneity. Similar values were found using the SISYFOS code, which predicts a homogeneity well above 90% (see Fig. 3).

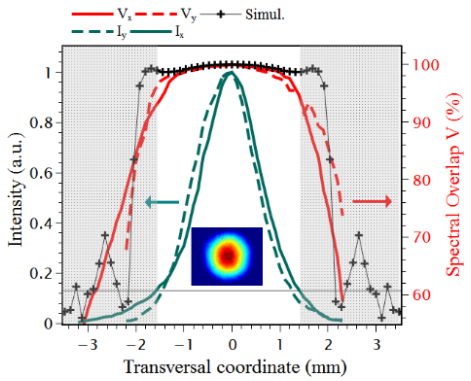

Fig. 3. Relative intensity (left axis) and spectral overlap V (right axis) across the beam profile along both transverse axes for the concave-convex configuration. Simulation (in black) using SISYFOS code. Indicative lines showing $1/e^2$ intensity level of the output beam.

3. Concave-concave setup

Even though the spectral homogeneity of the vex-cav system is comparable to those reported in other publications [3,4,22], we also set up a cav-cav configuration to make a direct comparison to this well-established geometry. The design goal was to find a cav-cav HC configuration providing the same broadening factor and enabling a compressed pulse duration of approximately 57 fs, comparable to the result obtained with the vex-cav geometry. Parameters such as the number of passes through the nonlinear material, the input pulse duration and energy, and the dispersion properties within the HC were preserved, as seen in Table 1. The cell length was adjusted accordingly to yield a similar eigenmode. Mirror M1 was the same in both experiments, but for the cav-cav configuration we replaced mirror M2a by mirror M2b with -250 mm ROC and a

Optics EXPRESS

highly reflective dielectric coating. The overall dispersion within the HC stayed approximately the same. The mirror separation was adjusted to 378 mm, which enabled the same 19 reflections per mirror and 38 passes through the nonlinear medium. The FS plate is placed at a distance d = 110 mm from M1. The Gaussian eigenmode of the cell is characterized by a beam radius of w_1 = 358 µm and w_2 = 471 µm on M1 and M2b respectively as well as w = 195 µm in the nonlinear material.

Fig. 4(a) shows the output beam spectrum. The spectrum spans from 990 nm to 1070 nm, with a corresponding FTL of 53 fs. Using the same dispersive mirror compressor with a total GDD compensation of -2400 fs^2, we achieve a compressed pulse duration of 57 fs FWHM, representing a pulse-shortening factor of 5. Some residual chirp is still present, similar to the previous case. Fig. 4(b) shows the FROG retrieved temporal pulse profile. A 90% overall transmittance through the HC was measured. The spectrum is once again predicted using the simulation code. The calculated spectral overlap for both axes and the corresponding prediction from the simulations is plotted in Fig. 5. The calculated effective overlaps for this configuration are V_x^{avg} = 99% and V_y^{avg} = 99%. These values are comparable to state-of-the-art measurements for spectral broadening in multipass systems. The spectral overlap parameter, $V_{x,y}^{avg}$, is a good indicator of the quality of the output beam. Increasing the nonlinearity, i.e., operating the cell using a B-integral above 0.6 rad per pass, leads to parameter values well below 90%, in the linear mode-matching regime. Larger nonlinearities can be attained by using non-linear mode matching, as shown in Viotti et al. [21], while preserving the output beam homogeneity.

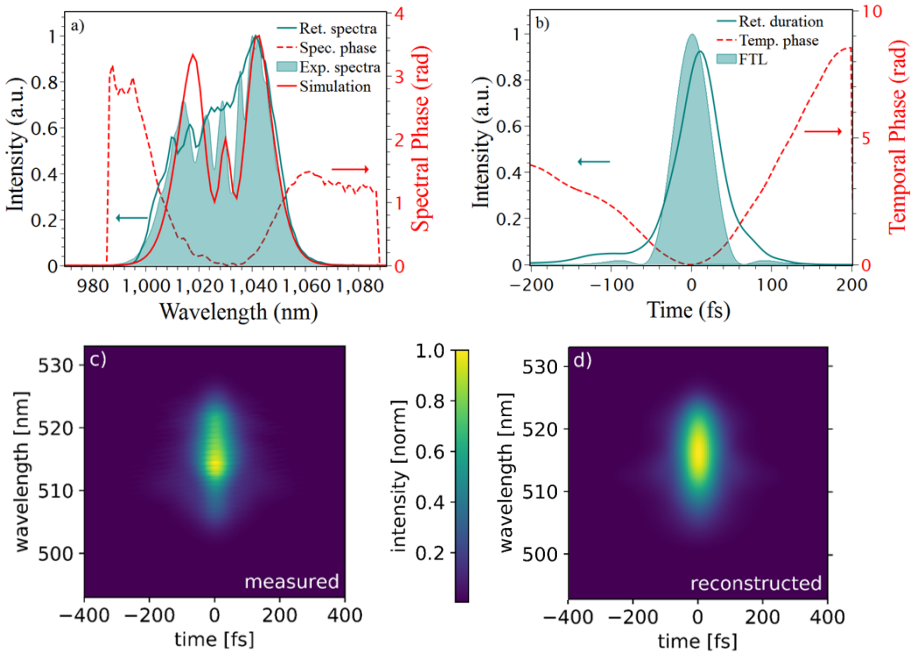

Fig. 4. a) Measured (shaded area), simulated (red line) and FROG-retrieved (green line) output spectrum and reconstructed spectral phase (dashed line) for the concave-concave configuration at an input energy of 15 µJ. The FROG error is 6×10^{-3} on a 256×256 grid. b) FROG-retrieved temporal profile (solid line), temporal phase profile (dashed line) and FTL reference (shaded area). Measured duration of 57 fs with a FTL of 53 fs. c) Measured and d) retrieved FROG traces.

Based on these measurements, the vex-cav configuration performs similarly to traditional cav-cav setups under the presented conditions. In either situation, the 260 fs input pulses were

Optics EXPRESS

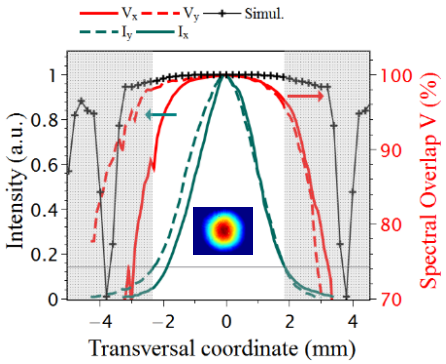

Fig. 5. Relative intensity (left axis) and spectral overlap V (right axis) across the beam profile along both transverse axes for the concave-concave configuration**.** Simulation (in black) using SISYFOS code. Indicative lines showing $1/e^2$ intensity level of the output beam.

compressed to ~50 fs with similar efficiencies (over 90%), which is in line with the design target and the data reported in the other publications. More remarkably, the overall homogeneity values V_x^{avg} and V_y^{avg} are both similar and above 98% and it is accurately predicted by the simulations. The proposed vex-cav broadening cell combines the excellent stability and robustness of HC-based systems while still maintaining the beam homogeneity.

4. Energy scaling in convex-concave multipass cells

Essentially, solid-state spectral broadening in cav-cav geometry is not limited by the input peak power and importantly by P_{peak}/P_{crit}. For example, previous demonstrations [2,14] showed P_{peak}/P_{crit} to be in the range 1-20 and even up to 1800 [23]. Importantly, the B-integral per pass should stay in the range of <0.6 rad to avoid any spatial beam deteriorations. Here we experimentally demonstrate that the same considerations apply to vex-cav configurations and show its operation in the regime $P_{peak}/P_{crit} = 200$ using a solid nonlinear medium. Moreover, we show that this novel configuration can be employed using gaseous media in the same fashion as the traditional cells with no loss in homogeneity. The setup consists of a concave mirror with a ROC of -1000 mm and a convex mirror of +3000 mm ROC both with 25.4 mm diameter, which allows an increased mode size inside the cell. The mirrors have a HR coating with no GDD compensation. The separation between them is only L = 283 mm yielding N = 13 bounces per mirror. The Gaussian eigenmode of the cell is characterized by a beam radius of w_1 = 497 μm on the concave mirror and w_2 = 402 μm on the convex mirror. Importantly, compared to cav-cav cells the eigenmode of vex-cav cell has only small variation of the beam diameter inside the cell. The maximum input energy into the cell was limited to 200 μJ out of a Light Conversion PHAROS laser.

The maximum input energy into the cell was limited to 200 μJ out of a Light Conversion PHAROS laser. The 260 fs long pulses were broadened in a solid medium or in gas in two separate experiments. In the first case, a 1 mm FS plate was placed 40 mm from the convex mirror. In the second case, the cell was filled with 7 bar of Argon. The input peak power is 720 MW resulting in a P_{peak}/P_{crit} ratio of 200 in case of the FS (~3.6 MW) and a ratio of 0.33 for the Argon. The compilation of the used parameters is presented in Table 2.

A B-integral per pass of approximately 0.5 rad was possible, in both cases, leading to a spectral coverage from 980 to 1070 nm as shown in Figure 6(a). An excellent homogeneity is preserved with both values V_x^{avg} and V_y^{avg} above 90% (Fig. 7(a)) and Fig. 8(a)), in the $1/e^2$ region, with the transmission over 93%. The evolution of the spectrum across the x-direction is shown in

Optics EXPRESS

Table 2. Experimental parameters for a Herriott-cell configuration, with either an FS plate or gas as nonlinear medium, for an input energy of 200 μJ.

Cell configuration	Eigenmode	Input pulse
R_1 -1000 mm	w_1 497 μm	E_p 200 μJ
R_2 + 3000 mm	w_2 402 μm	P_{peak} 7.2×10^8 W
L_{cell} 283 mm	w_{egn} 397 μm	τ_{fwhm} 260×10^{-15} s
M_{rt} 2	F_{peak} 7.9×10^{-2} J cm^{-2}	λ_0 1030 nm
N_{rt} 13	I_{peak} 2.6×10^{11} W cm^{-2}	P_{peak}/P_{crit} (FS) 200
η [%] 93	B_{int} ~0.5 rad	P_{peak}/P_{crit} (Ar) 0.33

Fig 7(b) and Fig. 8(b). Small changes in the spectrum are observed, however, these variations are expected and the spectrum preserves its general shape.

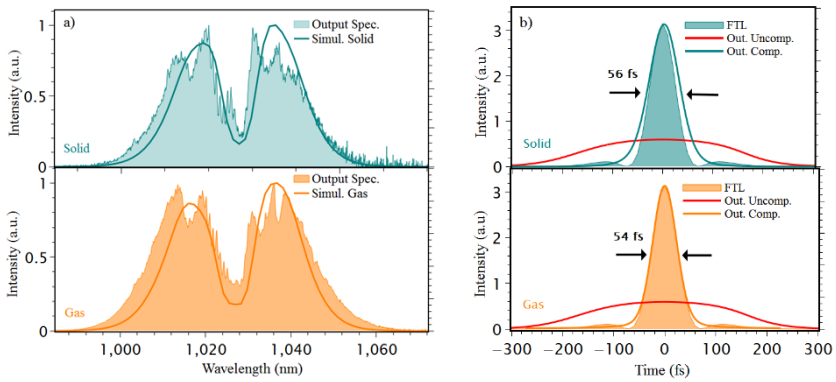

Fig. 6. a) Measured (shaded area) and simulated (solid line) output spectra for the vex-cav configuration at an input energy of 200 μJ, for solid- (top) and gas-based (bottom) broadening. b) Measured output duration and the respective FTL comparison for solid and gas media.

Once again, both the output spectrum and the homogeneity are well simulated using the SISYFOS code, assuming a nonlinear refractive index of $n_2 = 9.3 \times 10^{-23}$ m^2/W for Argon and the previously mention value for the FS plate. Only the nonlinear medium dispersion was considered (GVD (FS) = 18.97 fs^2/mm and GVD (Ar) = 0.016 fs^2/mm), assuming a flat phase from the mirror reflection. The simulations successfully predict the homogeneity values in the center of the laser beam profile, however the tails will present slightly larger experimental fluctuations than the simulations results. For the solid-based broadening, the cell was running in vacuum to avoid any influence of the ambient air. The output pulses were compressed to sub-60 fs, in both cases, using chirped mirrors delivering -3200 fs^2 of GDD. The output duration and the corresponding FTL are plotted in Fig. 6(b).

Optics EXPRESS

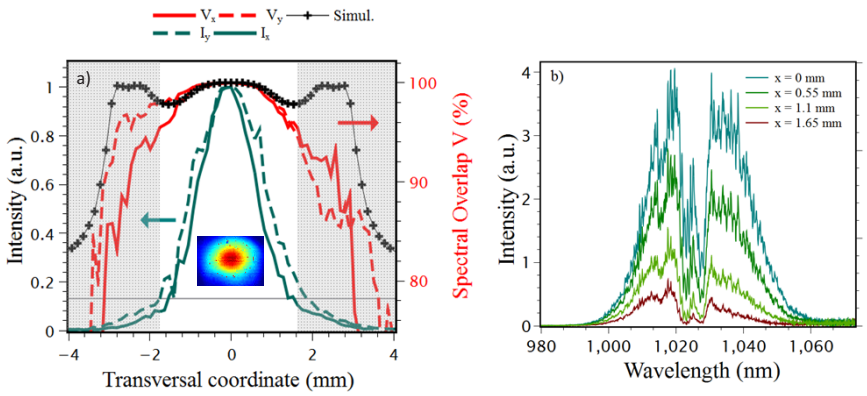

Fig. 7. Relative intensity (left axis) and spectral overlap V (right axis) across the beam profile along both transverse axes for the vex-cav configuration using 200µJ of input energy in case of 1 mm FS plate as nonlinear medium. Indicative lines showing $1/e^2$ intensity level of the output beam. Simulation, using SISYFOS code, of the spectral overlap across the radial profile shown in black. b) Spectra across the beam profile for different distances from the center.

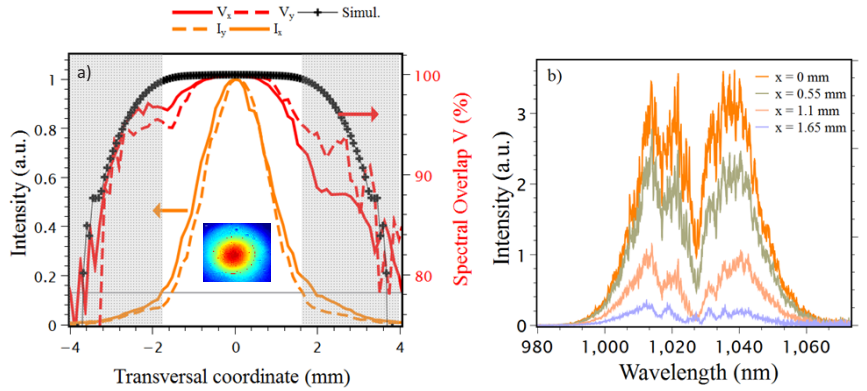

Fig. 8. Relative intensity (left axis) and spectral overlap V (right axis) across the beam profile along both transverse axes for the vex-cav configuration using 200µJ of input energy in case of 7 bar of Argon. Simulation, using SISYFOS code, of the spectral overlap across the radial profile shown in black. Indicative lines showing $1/e^2$ intensity level of the output beam. b) Spectra across the beam profile for different distances from the center.

Optics EXPRESS

5. Compact footprint for 40 mJ pulse broadening

For peak powers exceeding 1 GW, gas is commonly employed as a nonlinear medium. In previous publications [36,37] describing nonlinear broadening in cav-cav cell configurations and addressing sub-100-mJ-level energies, the damage threshold of the mirrors was found to be one of the peak power scaling limitations. In Kaumanns et al. [15], this limitation was circumvented by increasing the length of the cav-cav HC to 8 m, to enable 40 mJ input pulse energy in a 250 mBar argon atmosphere. This approach reduces the fluence on the mirrors by keeping a large spot size on their surface, although this is done at the cost of footprint. Moreover, while this approach can be employed to reduce the fluence on the cell mirrors, it directly leads to increased ionization effects in the focus, limiting the maximum allowed pulse energy for gas-based MPCs.

Here we propose an alternative vex-cav setup for the tens of millijoule energy range, with parameters summarized in Table 3. The mirrors have ROC of -30 m and +30 m, respectively, and they are separated by 4.1 m, allowing 46 passes through 500 mBar of Argon. The proposed setup could be implemented using 10×10 cm^2 cell mirrors. It is possible to predict the output spectrum and the beam spectral homogeneity using the previously mentioned code. The results are presented in Fig. 9. We predict an output spectrum spanning from 1010 nm to 1045 nm, supporting an FTL pulse of 76 fs, resulting in a compression factor of 17. The simulated broadening presents an excellent homogeneity, comparable to previously shown experimental results (above 90%). The evolution of the spectrum across the beam profile is shown in Fig. 9(c). Manufacturing mirrors with such a long radius of curvature can be challenging. The exact radius of curvature of the mirrors can be measured after the manufacturing, and the final cell configuration can be fine-tuned accordingly.

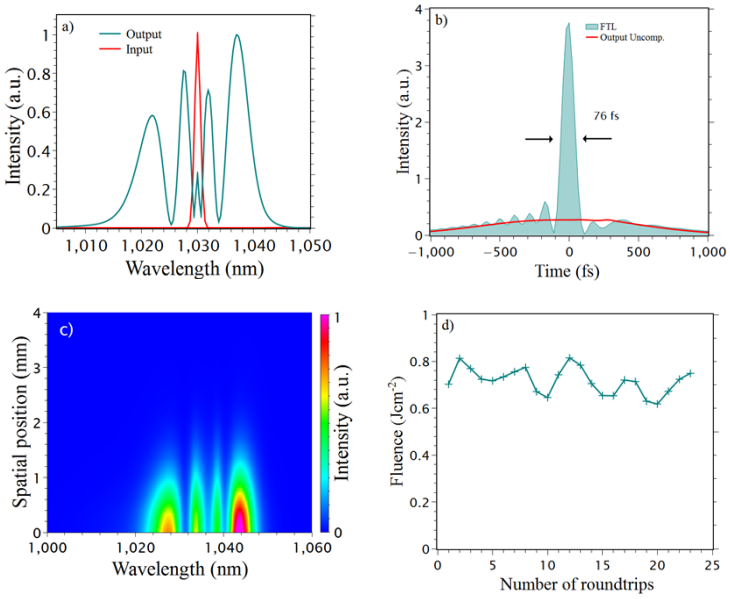

Fig. 9. a) Simulated output spectrum. b) Uncompressed output pulse duration and the Fourier transform limit. c) Spectral evolution across the beam profile showing excellent behavior. d) Fluence evolution on the convex mirror at each roundtrip.

The nominal design of the cell has a Gaussian eigenmode with 5.8 mm diameter on the convex mirror and a 6.8 mm diameter on the concave one, shown in Table 3. However, depending on the operation regime and using gas as nonlinear medium, for P_{peak}/P_{crit} ratios close to ~1, self-focusing effects need to be taken into account. In this case, to achieve the minimum fluence

Optics EXPRESS

Table 3. Proposed parameters for a Herriott-cell configuration for an input energy of 40 mJ.

Cell configuration	Eigenmode	Input pulse
R_1 -30.00 m	w_1 3.4 mm	E_p 40 mJ
R_2 30.00 m	w_2 2.9 mm	P_{peak} 2.9×10^{10} W
L_{cell} 4.1 m	w_{egn} 2.2 mm	τ_{fwhm} 1.3×10^{-12} s
M_{rt} 1	F_{peak} 0.3 J cm^{-2}	λ_0 1030 nm
N_{rt} 23	I_{peak} 2.1×10^{11} W cm^{-2}	P_{peak}/P_{crit} ~1
η [%] ~90	B_{int} 0.25 rad	P = 0.5 bar

on the convex mirror and small oscillations over all passes through the cell, Kerr nonlinearity is taken into consideration and a nonlinear mode-matching is necessary [30]. The method is described in more details in [30], and it is reached by adjusting the input beam size at the convex mirror plane. In particular, a beam diameter of 4.6 mm was used for this set of simulations. Using this approach, the evolution of the fluence on the convex mirror is shown in Fig. 9(d). A maximum fluence of 0.8 Jcm^{-2} for 40 mJ is predicted; however, this value is still below the laser damage threshold (F_{th}) for highly reflective mirrors in the picosecond range (1 Jcm^{-2}) [15]. The cell footprint is smaller than the traditional cav-cav geometry from [15]. Moreover, this setup offers the additional advantage of folding to even a smaller footprint, in a simple, elegant way similar to Cassegrain telescope geometry shown in Fig. 10. Multiple foldings are possible, converting large footprint systems into compact and less costly setups.

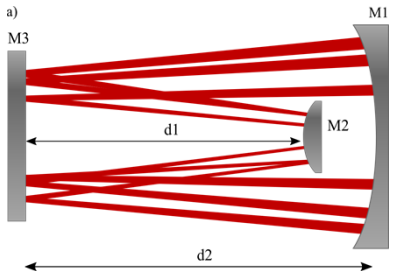

Fig. 10. Folding geometry for a concave-convex Herriott cell. The total distance between mirrors is given by d0 = d1 + d2.

Additionally, the convex-concave concept has been experimentally scaled to 2 mJ energy range and 2.9 GW peak power by using ambient air as a broadening medium [38]. In this case, pulses with P_{peak}/P_{crit} ratio of 0.6, were successfully compressed from 670 fs down to 134 fs with excellent spatio-spectral homogeneity.

Additional techniques can be employed to achieve even further scaling. Kaumanns et. al [24] and Huabao et. al. [39] showed that using first-order helical Laguerre–Gaussian modes can provide a solution for using peak powers above the critical power of the gaseous broadening media, without loss of the beam profile quality. Moreover, employing this technique at longer wavelengths could be beneficial. Material critical power has a quadratic dependence in wavelength, $P_{crit} \sim \lambda^2$, which allows further scaling in peak power for the same P_{peak}/P_{crit} ratio, avoiding self-focusing and laser breakdown in gas, which was numerically calculated in a multipass scheme based on vex-cav configuration by Hasting et. al. [40]. These additional techniques combined and further mirror ROCs scaling could provide a path toward J-level spectral broadening in a compact and efficient footprint.

Optics EXPRESS

6. Conclusion

In conclusion, we experimentally demonstrated and systematically studied a convex-concave configuration for the spectral broadening and compression of ultrashort pulses. In two proof-of-principle experiments, we demonstrated compression of pulses with 15 µJ and 200 µJ of energy from 260 fs to 50 fs at 15 W average power with an efficiency above 90%. Excellent spatio-spectral homogeneity of the output beam was measured for both solid- and gas-based broadening. The vex-cav multi-pass configuration extends the onset of SPM in air and the peak power limit for the broadening in the bulk material. We foresee that the main implication of the energy scaling concept will be the extension of spectral broadening and compression in high-energy range, circumventing the current gas ionization and optical damage threshold limitations.

Appendix A

For a general HC configuration the transfer matrix is given by:

$$T_{rt} = \begin{bmatrix} 1 & 0 \\ \frac{-2}{R_1} & 1 \end{bmatrix} \begin{bmatrix} 1 & L_{cell} \\ 0 & 1 \end{bmatrix} \begin{bmatrix} 1 & 0 \\ \frac{-2}{R_2} & 1 \end{bmatrix} \begin{bmatrix} 1 & L_{cell} \\ 0 & 1 \end{bmatrix} = \begin{bmatrix} -\frac{2L_{cell}-R_2}{R_2} & -\frac{2L_{cell}(L_{cell}-R_2)}{R_2} \\ \frac{2(2L_{cell}-R_2-R_1)}{R_2R_1} & \frac{4{L_{cell}}^2-4L_{cell}R_2-2L_{cell}R_1+R_2R_1}{R_2R_1} \end{bmatrix}$$

where L_{cell} is the length of the Herriott cell and $R_{1,2}$ are the respective ROCs of the mirrors.

The eigenmode is reproduced at each roundtrip through the cell and fulfills the condition:

$$T_{rt}(q_{eig}) = q_{eig} = \frac{A \cdot q_{eig} + B}{C \cdot q_{eig} + D}$$

$$q_{eig} = \frac{(A-D) \mp \sqrt{(A-D)^2 + 4BC}}{2C}$$

Here A, B, C, D are the elements of the matrix.

The eigen waist is calculated as:

$$w_{eig} = \left(\frac{L_{cell}\lambda_0}{\pi}\right)^{1/2} \left[-\frac{L_{cell}\,(L_{cell} - R_1)(L_{cell} - R_2)(L_{cell} - R_1 - R_2)}{-2{L_{cell}}^2R_1R_2 + L_{cell}\,{R_1}^2R_2 + L_{cell}R_1{R_2}^2}\right]^{1/4}$$

The waists on each mirror can be derived as:

$$w_1 = \left(\frac{L_{cell}\lambda_0}{\pi}\right)^{1/2} \left[\frac{g_2}{g_1(1-g_1g_2)}\right]^{1/4}$$

$$w_2 = \left(\frac{L_{cell}\lambda_0}{\pi}\right)^{1/2} \left[\frac{g_1}{g_2(1-g_1g_2)}\right]^{1/4}$$

With $g_{1,2}$ being:

$$g_{1,2} = 1 - \frac{L_{cell}}{R_{1,2}}$$

The Rayleigh length results as:

$$z_r^2 = w_{eig}^4\left(\frac{\pi}{\lambda_0}\right)^2 = \frac{L_{cell}\,(R_1 - L_{cell}\,)(R_2 - L_{cell}\,)(R_1 + R_2 - L_{cell}\,)}{(R_1 + R_2 - 2L_{cell})^2}$$

Optics EXPRESS

Appendix B

Starting by recognizing that for an optical setup with no change of environment, its transfer matrix has the det[T_{rt}] = 1 and that corresponds to the product of the eigenvalues of the matrix. It means that the eigenvalues are in the form :

$$\epsilon_{1,2} = \exp(\mp i\theta_{adv})$$

Here we can consider the θ_{adv}, as any real number.

Moreover, for any periodic optical system the re-entrant condition is given by:

$$T_{tot} = {T_{rt}}^{N_{rt}} = \begin{bmatrix} 1 & 0 \\ 0 & 1 \end{bmatrix}$$

Combining the above equations and knowing that the trace of the matrix is equal to the sum of the eigenvalues, it is possible to calculate:

$$tr[T_{rt}] = A + D = \epsilon_1 + \epsilon_2 = \exp(-i\theta_{adv}) + \exp(+i\theta_{adv}) = 2\cos(\theta_{adv})$$

From the Euler identity, for any number of roundtrips N_{rt}:

$${\epsilon_{1,2}}^{N_{rt}} = \exp(\mp i\theta_{adv}N_{rt}) = 1 \rightarrow \theta_{adv}N_{rt} = 2\pi M_{rt}, \qquad with\ M_{rt} \in \mathbb{N}_+$$

From this we derive that the angular advance θ_{adv}, is given by:

$$\theta_{adv} = \frac{2\pi M_{rt}}{N_{rt}},$$

and we can define M_{rt} as the cell configuration number.

This derivation is general and is valid for concave-convex and concave-concave cells and for any stable resonator configuration. The values of A and D of the transfer matrix are not limited, and the reentrance condition can be fulfilled. The ROC is negative for the convex mirrors. The length of cell and the angular advance only depend on the ROCs of the mirrors and the number of roundtrips N_{rt}.

Funding. Fundação para a Ciência e a Tecnologia (PD/BD/135222/2017).

Acknowledgments. This work is partially supported by the Fundação para a Ciência e a Tecnologia (grant agreement No. PD/BD/135222/2017). Considering the difficulty in setting up the new professorship in combination with typical university bureaucratic procedures, we sincerely acknowledge a few facilitators: A. Borchers, D. Kiesewetter, and A. Puckhaber.

Disclosures. The authors declare no conflicts of interest.

Data availability. Data underlying the results presented in this paper are not publicly available at this time but may be obtained from the authors upon reasonable request.

References

1. F. Albert, M. E. Couprie, and A. Debus, *et al.*, "Roadmap on plasma accelerators," New J. Phys. **23**(3), 031101 (2021).
2. J. Schulte, T. Sartorius, J. Weitenberg, A. Vernaleken, and P. Russbueldt, "Nonlinear pulse compression in a multi-pass cell," Opt. Lett. **41**(19), 4511–4514 (2016).
3. J. Weitenberg, T. Saule, J. Schulte, and P. Rusbuldt, "Nonlinear Pulse Compression to Sub-40 fs at 4.5 µJ Pulse Energy by Multi-Pass-Cell Spectral Broadening," IEEE J. Quantum Electron. **53**(6), 1–4 (2017).
4. J. Weitenberg, A. Vernaleken, J. Schulte, A. Ozawa, T. Sartorius, V. Pervak, H.-D. Hoffmann, T. Udem, P. Russbüldt, and T. W. Hänsch, "Multi-pass-cell-based nonlinear pulse compression to 115 fs at 7.5 µJ pulse energy and 300 W average power," Opt. Express **25**(17), 20502–20510 (2017).
5. J. in Kim, Y. G. Kim, J. M. Yang, J. W. Yoon, J. H. Sung, S. K. Lee, and C. H. Nam, "Sub-10 fs pulse generation by post-compression for peak-power enhancement of a 100-TW Ti:Sapphire laser," Opt. Express **30**(6), 8734–8741 (2022).

Optics EXPRESS

6. S. Y. Mironov, S. Fourmaux, P. Lassonde, V. N. Ginzburg, S. Payeur, J.-C. Kieffer, E. A. Khazanov, and G. Mourou, "Thin plate compression of a sub-petawatt Ti:Sa laser pulses," Appl. Phys. Lett. **116**(24), 241101 (2020).
7. V. Ginzburg, I. Yakovlev, A. Zuev, A. Korobeynikova, A. Kochetkov, A. Kuzmin, S. Mironov, A. Shaykin, I. Shaikin, E. Khazanov, and G. Mourou, "Fivefold compression of 250-TW laser pulses," Phys. Rev. A **101**(1), 013829 (2020).
8. E. A. Khazanov, S. Y. Mironov, and G. Mourou, "Nonlinear compression of high-power laser pulses: compression after compressor approach," Phys.-Usp. **62**(11), 1096–1124 (2019).
9. A. Suda, M. Hatayama, K. Nagasaka, and K. Midorikawa, "Generation of sub-10-fs, 5-mJ-optical pulses using a hollow fiber with a pressure gradient," Appl. Phys. Lett. **86**(11), 111116 (2005).
10. G. Fan, P. A. Carpeggiani, Z. Tao, G. Coccia, R. Safaei, E. Kaksis, A. Pugzlys, F. Légaré, B. E. Schmidt, and A. Baltuška, "70 mJ nonlinear compression and scaling route for an Yb amplifier using large-core hollow fibers," Opt. Lett. **46**(4), 896–899 (2021).
11. M. Hentschel, R. Kienberger, C. Spielmann, G. A. Reider, N. Milosevic, T. Brabec, P. Corkum, U. Heinzmann, M. Drescher, and F. Krausz, "Attosecond metrology," Nature **414**(6863), 509–513 (2001).
12. A.-L. Viotti, M. Seidel, E. Escoto, S. Rajhans, W. P. Leemans, I. Hartl, and C. M. Heyl, "Multi-pass cells for post-compression of ultrashort laser pulses," Optica **9**(2), 197 (2022).
13. T. Nagy, P. Simon, and L. Veisz, "High-energy few-cycle pulses: post-compression techniques," Adv. Phys.: X 6, (2021).
14. K. Fritsch, M. Poetzlberger, V. Pervak, J. Brons, and O. Pronin, "All-solid-state multipass spectral broadening to sub-20 fs," Opt. Lett. **43**(19), 4643–4646 (2018).
15. M. Kaumanns, V. Pervak, D. Kormin, V. Leshchenko, A. Kessel, Y. Chen, and T. Nubbemeyer, eds., *Multipass spectral broadening with tens of millijoule pulse energy* (Optical Society of America, 2019).
16. M. Ueffing, S. Reiger, M. Kaumanns, V. Pervak, M. Trubetskov, T. Nubbemeyer, and F. Krausz, "Nonlinear pulse compression in a gas-filled multipass cell," Opt. Lett. **43**(9), 2070–2073 (2018).
17. S. N. Vlasov, E. V. Koposova, and V. E. Yashin, "Spectral broadening and compression of high-intensity laser pulses in quasi-periodic systems with Kerr nonlinearity," Quantum Electron. **42**(11), 989–995 (2012).
18. S. Goncharov, K. Fritsch, and O. Pronin, "Few-cycle pulse compression and white light generation in cascaded multipass cells," Opt. Lett. **48**(1), 147–150 (2023).
19. P. Balla, A. Bin Wahid, and I. Sytcevich, *et al.*, "Postcompression of picosecond pulses into the few-cycle regime," Opt. Lett. **45**(9), 2572–2575 (2020).
20. S. Hädrich, E. Shestaev, and M. Tschernajew, *et al.*, "Carrier-envelope phase stable few-cycle laser system delivering more than 100 W, 1 mJ, sub-2-cycle pulses," Opt. Lett. **47**(6), 1537–1540 (2022).
21. A.-L. Viotti, C. Li, G. Arisholm, L. Winkelmann, I. Hartl, C. M. Heyl, and M. Seidel, "Few-cycle pulse generation by double-stage hybrid multi-pass multi-plate nonlinear pulse compression," Opt. Lett. **48**(4), 984–987 (2023).
22. M. Kaumanns, V. Pervak, D. Kormin, V. Leshchenko, A. Kessel, M. Ueffing, Y. Chen, and T. Nubbemeyer, "Multipass spectral broadening of 18 mJ pulses compressible from 1.3 ps to 41 fs," Opt. Lett. **43**(23), 5877–5880 (2018).
23. Reimund Martin Kaumanns, "Generation of Energetic Femtosecond Pulses at High Average Power," (2020); Ph.D. thesis (Ludwig Maximilian University of Munich).
24. M. Kaumanns, D. Kormin, T. Nubbemeyer, V. Pervak, and S. Karsch, "Spectral broadening of 112 mJ, 13 ps pulses at 5 kHz in a donut mode multipass with compressibility to 37 fs," Opt. Lett. **46**(5), 929 (2021).
25. M. Hanna, X. Délen, L. Lavenu, F. Guichard, Y. Zaouter, F. Druon, and P. Georges, "Nonlinear temporal compression in multipass cells: theory," J. Opt. Soc. Am. B **34**(7), 1340 (2017).
26. W. Koechner, *Solid-State Laser Engineering* (Springer New York; Springer e-books, 2006).
27. Oleg Pronin, Kilian Fritsch, and Victor Hariton, "Vorrichtung zur spektralen Verbreiterung eines Laserimpulses und Lasersystem," Patent EP 2021/062702, 2021 (2021).
28. Gunnar Arisholm and Helge Fonnum, "Simulation System For Optical Science (SISYFOS) - tutorial, version 2," (2021).
29. M. Seidel, X. Xiao, and A. Hartung, "Solid-Core Fiber Spectral Broadening at Its Limits," IEEE J. Select. Topics Quantum Electron. **24**(5), 1–8 (2018).
30. M. Seidel, P. Balla, C. Li, G. Arisholm, L. Winkelmann, I. Hartl, and C. M. Heyl, "Factor 30 Pulse Compression by Hybrid Multipass Multiplate Spectral Broadening," Ultrafast Science **2022**, 1–10 (2022).
31. C. M. Heyl, M. Seidel, E. Escoto, A. Schönberg, S. Carlström, G. Arisholm, T. Lang, and I. Hartl, "High-energy bow tie multi-pass cells for nonlinear spectral broadening applications," J. Phys. Photonics **4**(1), 014002 (2022).
32. Claude Rolland and P. B. Corkum, "Compression of high-power optical pulses," J. Opt. Soc. Am. B **5**(3), 641–647 (1988).
33. M. Seidel, G. Arisholm, J. Brons, V. Pervak, and O. Pronin, "All solid-state spectral broadening: an average and peak power scalable method for compression of ultrashort pulses," Opt. Express **24**(9), 9412–9428 (2016).
34. J. Brons, "High-power femtosecond laser-oscillators for applications in high-field physics," Diss. Ludwig Maximilians Universität München, 2017.
35. T. Brabec and F. Krausz, "Nonlinear Optical Pulse Propagation in the Single-Cycle Regime," Phys. Rev. Lett. **78**(17), 3282–3285 (1997).
36. L. Lavenu, M. Natile, F. Guichard, X. Délen, M. Hanna, Y. Zaouter, and P. Georges, "High-power two-cycle ultrafast source based on hybrid nonlinear compression," Opt. Express **27**(3), 1958–1967 (2019).

Optics EXPRESS

37. P. Russbueldt, J. Weitenberg, J. Schulte, R. Meyer, C. Meinhardt, H. D. Hoffmann, and R. Poprawe, "Scalable 30 fs laser source with 530 W average power," Opt. Lett. **44**(21), 5222 (2019).
38. A. Omar, T. Vogel, M. Hoffmann, and C. J. Saraceno, "Spectral broadening of 2-mJ femtosecond pulses in a compact air-filled convex-concave multi-pass cell," Opt. Lett. **48**(6), 1458–1461 (2023).
39. Huabao Cao, Roland S. Nagymihaly, and Mikhail Kalashnikov, "Relativistic near-single-cycle optical vortex pulses from noble gas-filled multipass cells," Opt. Lett. **45**(12), 3240–3243 (2020).
40. M. G. Hastings, P. Panagiotopoulos, M. Kolesik, V. Hasson, S. Tochitsky, and J. V. Moloney, "Few-cycle 10 μm multi-terawatt pulse self-compression in a gas-filled multi-pass cell: a numerical experiment," J. Opt. Soc. Am. B **39**(1), 266 (2022).